J. Fluid Mech. (1995), *vol.* 284, *pp.* 1–21

Mixing induced by oscillatory stratified flow past a right-circular cylinder

By M. J. A. M. PERERA, H. J. S. FERNANDO AND D. L. BOYER

Environmental Fluid Dynamics Program *and* Department of Mechanical and Aerospace Engineering, Arizona State University, Tempe, AZ 85287-6106, USA

(Received 23 February 1993 and in revised form 4 August 1994)

A series of laboratory experiments was performed to investigate the overall mixing characteristics of oscillatory stratified flow past an isolated topography. The experiments were conducted by oscillating a right-circular cylinder in an otherwise quiescent linearly stratified fluid contained in a rectangular basin. The mixing was largely confined to the turbulent 'core' region around the cylinder. This mixed fluid was then injected into the fluid interior of the basin by numerous intrusive tongues. These intrusions were accompanied by return currents of unmixed stratified fluid into the turbulent core. The overall effect of this mixing process was to increase the potential energy of the fluid in the basin. An expression is derived to relate the rate of change of potential energy of the system to the basin-averaged buoyancy flux. This formula was then used to calculate the mean buoyancy flux from measurements of the rate of change of potential energy of the fluid system. Basin-averaged diapycnal eddy diffusivities for the experiments were evaluated and the results were found to be in good agreement with the predictions of a heuristic model based on the energetics of the mixing. Observations on the spreading of intrusions and the evolution of the density field are also presented.

1. Introduction

An understanding of the vertical transport of heat and salt in natural water masses is important in evaluating the balances of such quantities as heat, salt and biological matter. Because of the limited spatial resolution of existing general circulation models, accurate parameterization of small-scale diapycnal mixing processes, in particular horizontal and vertical eddy diffusivities, are required to effect the closure of the governing equations. The reliability of such parameterizations depends on: (i) how accurately the mixing mechanisms, the resulting fluxes, and their spatial and temporal intermittency are known; and (ii) the versatility of the turbulence models employed. In the open ocean, many mechanisms have been suggested as potential mixing agents; these include, Kelvin–Helmholtz shear instabilities, convective breaking of internal waves (Thorpe 1987), double diffusion (Turner 1985), critical-layer absorption (Dillon *et al.* 1989) and surface-stress-driven mixing. In addition, there is evidence for the presence of extremely powerful, yet rare, mixing events within isolated regions known as convective chimneys (Killworth 1976), which may account for the entire bottom (deep) water formation of the oceans.

Various parameterizations are available for small-scale open ocean mixing, with the most recent one being due to Gregg (1989) who proposed a semi-empirical relationship between the dissipation of turbulent kinetic energy and the shear variance at vertical wavenumbers less than 0.1 c.p.m. However, such approaches are of limited value when

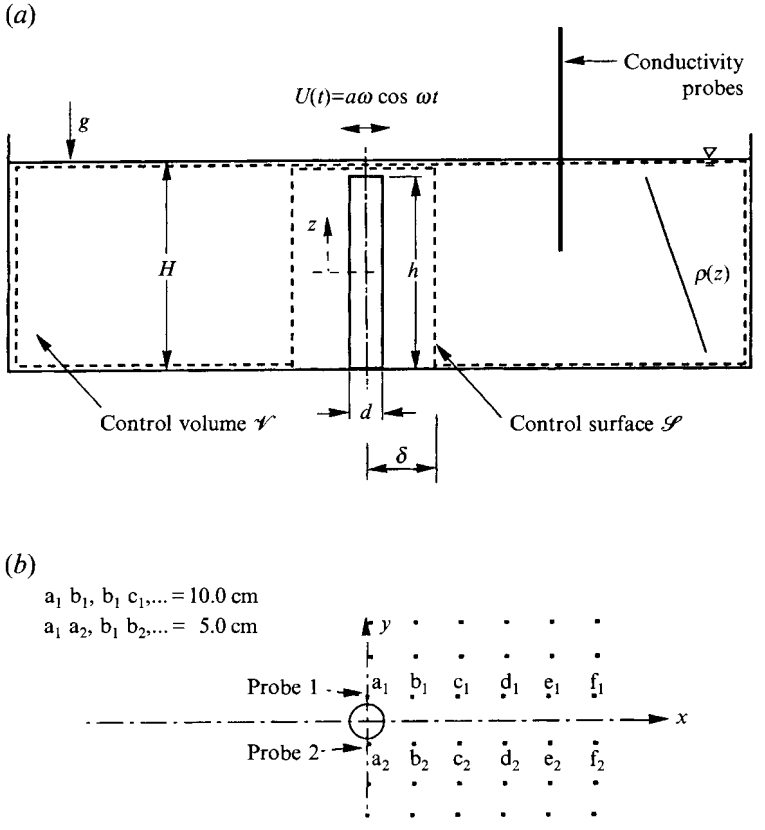

FIGURE 1. (*a*) A schematic diagram of the experiment. (*b*) The locations where vertical conductivity probe traverses were made.

considering mixing in the presence of ocean boundaries such as continental slopes, seamounts and guyots, although sometimes deep ocean parameterizations have been used for littoral waters. For example, D'Asaro & Morison (1992) employed Gregg's (1989) model to show that vertical mixing in the Arctic Ocean is dominated by steep topographical features. As suggested by Munk (1966), and later investigated by many workers (for example, see Garrett, MacCready & Rhines 1993 for a review), intense turbulence generated near topographic features can enhance considerably oceanic diapycnal mixing. In the laboratory context, this was demonstrated by Ivey & Corcos (1982) and Thorpe (1982), who generated an isolated turbulent mixed layer near the boundaries of a stratified fluid. Most diapycnal mixing was found to occur within the turbulent region; the collapse of turbulence at its edge was found to generate a series of intrusions which carried mixed fluid into the non-turbulent interior of the basin. This work has been extended to include inclined boundaries by Phillips, Shyu & Salmun (1986) and Salmun & Phillips (1992). There are useful analyses on the possibility of enhanced or damped mixing at sloping boundaries in Garrett (1989, 1991), Woods (1991), Salmun, Killworth & Blundell (1991) and Imberger & Ivey (1993).

As suggested by Stommel & Arons (1960), in studying vertical mixing induced by isolated topographic features such as seamounts, it is useful to express the contribution of overall mixing in terms of a single vertical basin-scale eddy diffusivity. Flow and mixing at a topography are extremely complex and isolation of contributions from

individual mechanisms is difficult. Internal wave reflection (Eriksen 1982), topographically trapped waves (Brink 1990), Taylor columns (Roden & Taft 1985), bottom intensification (Eriksen, as quoted by Roden 1991), eddy shedding, and interaction between vortices and rotating wake structures (Roden 1991) all contribute to the complexity.

The aim of the present work is to carry out a series of laboratory experiments dealing with mixing at isolated topographies. As a first step, a steep topography (cylinder) of height h and horizontal dimension d, submerged in a linearly stratified fluid of buoyancy frequency N, was used. No background rotation was considered. The turbulence was generated by oscillating the topography with a frequency ω and amplitude a; see figure 1. This enabled one to study the mixing induced by the oscillatory flow component only. To our knowledge no such experiments dealing with mixing at isolated topographies have been reported previously. A background flow consisting of a pure oscillation is a reasonable approximation for the motion field in the vicinity of isolated seamounts as found in recent field studies. For example, Roden (1991) reports that the mean component near Fieberling Guyot is 1 cm s^{-1} compared to an oscillatory flow amplitude of 48 cm s^{-1}. Similar observations have been reported by Ozmidov (1990) for Ampere seamount. In these areas, the background flow is a superposition of randomly moving eddies (whose origin is not very well known) and tidal contributions.

In §2, the experimental procedure is discussed. The theoretical aspects of the evaluation of basin-averaged eddy diffusivity, together with a simple model to predict it for the case of oscillatory flow past a right-circular cylinder, are discussed in §3. Experimental observations and measurements are discussed in §§4 and 5, respectively. A summary of the salient findings is given in §6 and a discussion of the study is presented in §7.

2. Experiments

The experiments were carried out in a Plexiglas tank with dimensions 0.2 m deep, 0.4 m wide and 1.25 m long, filled to a depth of 0.17 m with a linearly stratified brine solution; see figure 1(*a*). A vertical cylinder was attached to a thin wire at its bottom, and was oscillated laterally via an eccentric crank and two arm links. Cylinders of diameter 2.6, 3.2, 3.9 cm and height 8.0, 9.8, 14.0 cm were used. The crank radius was adjustable, but a typical ratio of arm length to crank radius was about 15; this yielded a good approximation to a simple sinusoidal motion. The oscillation frequency and amplitude were varied in the ranges, 17–30 rad s^{-1} and 1–1.5 cm, respectively.

Density measurements were obtained using a four-electrode micro-scale conductivity probe designed and tested by Precision Measurements Inc.; see Head (1983). Six conductivity probes were attached to a precision traversing mechanism driven by a screw-shaft connected to a stepping motor. The traversing speed could be varied from 0.5 to 30 cm s^{-1}. The traversing mechanism was mounted on a carriage placed on parallel rails bolted to the top of the tank. The carriage enabled the computer-controlled positioning of the probes at any location in the longitudinal and transverse directions of the tank. The vertical position of the probes was recorded with the aid of a rotary potentiometer, geared to the driving motor.

The output from the potentiometer and the six conductivity probes were acquired via an A/D converter (Metrabyte, DAS-16G2) and a computer. Because the variation between successive conductivity profiles is small, it was necessary to use 12-bit resolution for data acquisition. The resulting conductivity traces with depth were

converted to density versus depth records by calibrating against a range of solutions of known density, as discussed below.

Samples of known density, in steps of 0.005 gm cm^{-3}, were prepared from 1.00 to 1.03 gm cm^{-3}. A Baum hydrometer was used for the density measurements. The conductivity probes were immersed in samples, and the voltage readings were acquired via the DAS-16G2, from which the calibration curves were prepared. Over the calibration period, the density calculated was within an accuracy of 1 % of the average. The potentiometer was calibrated in steps of 1 cm by tracking the movement of the carriage against a standard scale.

The density stratification in the tank was established using common salt (sodium chloride), by employing the two-tank technique of Fortuin (1960). The tank was filled from the bottom by using two flat diffusers (which release fluid as a horizontal sheet) attached at the centre of both ends of the tank to prevent mixing. The fluid was allowed to settle for about two hours before commencing the experiments. The initial buoyancy frequency was approximately uniform and was varied between 0.6 and 1.5 rad s^{-1}. The experimental arrangement enabled the variation of the ambient density stratification N, the oscillating cylinder frequency ω, the oscillation amplitude a and the cylinder diameter d. In all of the experiments, the height of the cylinder was maintained at $h \leqslant 14$ cm while the fluid level $H = 17$ cm was kept constant. The use of $h > 14$ cm resulted in surface waves and thus was not utilized. The cylinder Reynolds number, defined as $Re_c = (a\omega)\, d/\nu$, was of the order of 10^4. Fast conductivity traverses through the mixed layer near the cylinder indicated the presence of density overturns, suggesting that the cylinder wake was turbulent. Flow visualization was accomplished by means of shadowgraphs and dye tracers (e.g. fluorescein).

The cylinder oscillations were continued for about 25 to 30 minutes for each experiment. The fluid was then allowed to come to a quasi-equilibrium state by waiting 5–10 minutes before measuring the final density profiles. (Although at such times the intrusions appear to be stationary, it is expected that the interleaving intrusions evolve over very large timescales because of the residual horizontal gradients. At such large times, however, molecular diffusion processes, unrelated to boundary mixing, become important.) This enabled the mixed parcels of fluid formed during mixing to settle at their neutral levels.

A detailed error analysis was made on the measured results using the approach given in Coleman & Steele (1989); this was necessary in view of the difficulties due to the subtraction of two large quantities to obtain the buoyancy flux, a rather small quantity; see §4. The uncertainty of the non-dimensional vertical eddy diffusivity was calculated as $\pm 11\,\%$.

3. Theoretical considerations

3.1. *Calculation of the buoyancy flux*

Consider a quiescent, linearly stratified fluid to initially occupy a rectangular box of dimensions $L_x \times L_y \times H$; see figure 1. At time $t = 0$, a right circular cylinder, oriented as shown, is forced to oscillate sinusoidally in the x-direction, where the rectangular Cartesian coordinates x, y, z are fixed to the tank. The initial density distribution is characterized by a mean density ρ_0 and density difference from bottom to top $\Delta\rho$. It is desired to investigate the mixing process as effected by the cylinder.

The mixing is effectively taking place in the turbulent boundary layer surrounding the cylinder, and the mixed fluid is advected to the non-turbulent stratified interior by a series of interleaving intrusions, driven by horizontal pressure gradients. The return

currents that are set up between the intrusions feed unmixed fluid from the interior to the turbulent region; this tends to restore the stratification on which further mixing can act. This process can continue until the interior stratification is completely destroyed. The nature of these layered intrusive/return flows is clearly seen in the flow visualization pictures presented by Browand, Guyomar & Yoon (1987) who used horizontally oscillating vertical grids to study turbulent mixing in stratified fluids. Obtaining statistical measures of such flows is extremely difficult, owing to their being both horizontally and vertically inhomogeneous. As such, in this investigation, we seek information only on bulk mixing characteristics, which in turn requires measurements of overall buoyancy transfer characteristics of the system. In calculating the volume-averaged buoyancy flux, the following procedure was adopted.

The average potential energy of the tank at a given time t can be written as

$$\lambda(t) = \int_{-H/2}^{H/2} \int_{-L_y/2}^{L_y/2} \int_{-L_x/2}^{L_x/2} \bar{\rho}(x, y, z, t)\, gz \, \mathrm{d}x \, \mathrm{d}y \, \mathrm{d}z, \tag{3.1}$$

where ρ is the density (overbar denotes the mean) and g the gravitational acceleration. The rate of change of potential energy λ of the system thus becomes

$$\frac{\mathrm{d}\lambda}{\mathrm{d}t} = \iiint_V \frac{\partial \bar{\rho}}{\partial t} gz \, \mathrm{d}x \, \mathrm{d}y \, \mathrm{d}z = -\rho_0 \iiint_V \frac{\partial \bar{b}}{\partial t} z \, \mathrm{d}x \, \mathrm{d}y \, \mathrm{d}z = -\rho_0 \iiint_V (\boldsymbol{\nabla} \cdot \boldsymbol{q}) z \, \mathrm{d}x \, \mathrm{d}y \, \mathrm{d}z, \tag{3.2}$$

where we have used the definition of buoyancy

$$b = -\frac{\rho - \rho_0}{\rho_0} g, \tag{3.3}$$

and the conservation law of buoyancy in the absence of a mean flow,

$$\frac{\partial \bar{b}}{\partial t} = \boldsymbol{\nabla} \cdot \boldsymbol{q}, \tag{3.4}$$

where $\boldsymbol{q} = k \boldsymbol{\nabla} \bar{b} - \overline{b' \boldsymbol{u}}$ is the buoyancy flux, k is the molecular diffusivity, $\boldsymbol{u}$ is the velocity, b' is the fluctuation of buoyancy and $V (= L_x L_y H)$ is the volume defined by the limits in (3.1); owing to the short timescales considered, the molecular-diffusive flux can be neglected. The reference density in (3.3) can be defined as

$$\rho_0 = \frac{1}{L_x L_y H} \iiint_V \rho(x, y, z, t) \, \mathrm{d}x \, \mathrm{d}y \, \mathrm{d}z = \rho(x, y, 0, 0) \tag{3.5}$$

because of the linearity of the initial stratification. After integration of (3.2), and using the no-flux condition at the basin boundaries, one obtains

$$\Lambda = \frac{\mathrm{d}\lambda}{\mathrm{d}t} = \rho_0 V \langle q_3 \rangle, \tag{3.6}$$

where $\rho_0 V$ is the mass of the fluid in the container, $q_3 = \overline{b' u_3}$ is the vertical buoyancy flux, u_3 is the vertical velocity fluctuation, and the angle brackets represent the volume-averaged value, defined as

$$\langle q_i \rangle = \frac{1}{L_x L_y H} \iiint_V -(\overline{b' u_i}) \, \mathrm{d}x \, \mathrm{d}y \, \mathrm{d}z. \tag{3.7}$$

Thus, as is evident from (3.6), the volume-averaged buoyancy flux due to mixing caused by the obstacle can be measured by the change of potential energy of the system during a given time. By adapting the definition (see, for example, Osborn 1980)

$$\kappa = -\overline{b'u_3}/\mathrm{d}\bar{b}/\mathrm{d}z, \tag{3.8}$$

the basin-averaged eddy diffusivity κ can be calculated using the measured rate of change of potential energy as

$$\kappa = \frac{\Lambda}{\rho_0 V N^2}. \tag{3.9}$$

The techniques adopted to measure κ are described in §4.

3.2. *A simple model for eddy diffusivity*

In order to develop a framework for the interpretation of the experimental results, it is instructive to construct a simple model to predict the vertical eddy diffusivity of oscillatory flow past a topography. In so doing, hypothesize that the topography acts as a turbulent energy source for the stratified region, which raises its potential energy uniformly as a consequence of turbulent mixing. Obviously, this is a simplified picture of the mixing taking place near the topography, i.e. the feeding of mixed fluid into the non-turbulent stratified region as interleaving intrusions and the replenishment of mixed fluid in the turbulent boundary layer by stratified return currents. In reality, there is no turbulent interior, and the concept of eddy diffusivity is inapplicable in a strictly local sense. However, the interest here is to parameterize the increase in the potential energy in the interior as a result of boundary mixing using a volume-averaged diffusivity. In view of the macroscopic (volume-averaged) nature of the present analysis, this simplified approach is thought to be reasonable.

Isolate the turbulence source by a control surface $\mathscr{S}$ (figure 1*a*). In the model, it is hypothesized that the turbulent kinetic energy available for mixing is 'diffused' into the outer stratified region (or basin interior) contained in the control volume $\mathscr{V}$ and causes mixing in the interior of the fluid. (Note that the basin interior is not turbulent but undergoes changes in density gradient.) A region of radius δ surrounding the topography and encompassing the turbulent boundary layer essentially separates the turbulent and non-turbulent regions. Assuming that the turbulent energy diffused through the surface $\mathscr{S}$ is responsible for mixing within $\mathscr{V}$, one can write the turbulent kinetic energy equation for $\mathscr{V}$ as

$$-\frac{\partial M_j}{\partial x_j} - q_3 - \epsilon \approx 0, \tag{3.10}$$

where M_j is the turbulent energy flux, ϵ is the rate of dissipation of turbulent kinetic energy and quasi-stationary conditions are assumed. Integrating (3.10) over the control volume $\mathscr{V}$, and considering the boundary flux of turbulent kinetic energy through $\mathscr{S}$, one obtains

$$\int_{\mathscr{S}} M_j n_j \,\mathrm{d}\mathscr{S} \approx -\int_{\mathscr{V}} (q_3 + \epsilon)\,\mathrm{d}\mathscr{V}, \tag{3.11}$$

where n_j is the unit vector perpendicular to $\mathscr{S}$. Assuming a constant mixing efficiency of η for this forced stratified turbulent flow, one obtains

$$\int_{\mathscr{S}} M_j n_j \,\mathrm{d}\mathscr{S} \approx -\frac{1}{\eta}\int q_3 \,\mathrm{d}\mathscr{V} = \frac{V}{\eta}\langle q_3 \rangle \approx -\kappa N^2 \frac{L_x L_y H}{\eta}, \tag{3.12}$$

where $\eta = q_3/(q_3+\epsilon)$, and the first term represents the total turbulent energy crossing the boundary $\mathscr{S}$, which is available for mixing. (The approach here is somewhat similar to that used by McEwan 1983 in evaluating mixing efficiency in a fluid column by breaking internal waves.) Assuming that the velocity fluctuations in the turbulent layer (of width δ) can be parameterized by $(a\omega)$ and that $\delta/h \ll 1$, it is possible to parameterize

$$\int_{\mathscr{S}} M_j n_j \, \mathrm{d}\mathscr{S} \sim -(a\omega)^3 2\pi\delta h, \tag{3.13}$$

which, when combined with (3.12), gives

$$\frac{\kappa}{d^2 N} = \alpha Ri^{-3/2}\left(\frac{d}{H}\right)\left(\frac{\delta h}{L_x L_y}\right), \tag{3.14}$$

where α is a constant and Ri is a bulk Richardson number defined by

$$Ri = \frac{N^2 d^2}{a^2\omega^2}. \tag{3.15}$$

Note that in (3.14), the dependence of κ on the cylinder diameter d is implicitly included by way of the boundary-layer width δ. The normalization for κ and the definition of Ri are based on d because of its influence in determining the turbulent scales in the boundary layer and as a representative quantity of the scale of the topography.

3.3. *Dimensional analysis*

Another way of assimilating the experimental data is to directly use dimensional analysis. To this end, assume that

$$\kappa = \kappa(\omega, a, d, N, h, L_x, L_y, H). \tag{3.16}$$

A notable omission from (3.16) is the kinematic viscosity of the fluid ν. This is due to the assumption that the turbulent mixing is sufficiently strong that Reynolds-number effects are unimportant and that horizontal adjustments due to buoyancy anomalies are independent of viscous effects. (This is corroborated by the results of (5.5).) Thus, (3.16) can be written as

$$\frac{\kappa}{d^2 N} = f\left(\frac{\omega}{N}, \frac{a}{d}, \frac{d}{h}, \frac{h}{L_x}, \frac{h}{L_y}, \frac{h}{H}\right), \tag{3.17}$$

where f is a function.

Because a tank of given dimensions was used to perform the experiments and owing to practical constraints on investigating the effects of variable h/H, it was not possible to systematically investigate the dependence of κ/d^2N on the last three parameters. Thus, to put the results in perspective in terms of non-dimensional variables, it is instructive to use the form (3.14). This requires parameterization of the horizontal turbulent boundary-layer width δ in terms of governing parameters. Intuitively one expects δ to depend on a, d, ω and N, and to be insensitive to variations in h, H, L_x and L_y. To this end, the formula proposed by Thorpe (1982) is of use; accordingly the thickness of the boundary layer generated by horizontal oscillations of a vertical grid in a linearly stratified fluid should take the form

$$\delta = \beta a^{3/4} M^{1/4}\left(\frac{\omega}{N}\right)^{1/2}, \tag{3.18}$$

where M is the mesh size of the stirring grid used and β is a constant. Measurements obtained using shadowgraph flow visualization of the boundary layer indicate that (3.18) is a good approximation for the present experiments when $\beta \approx 1.30$ and when M of the grid of (3.18) is replaced by the diameter of the cylinder d. It is also interesting to note that the vertical thickness of the intrusions (say ζ) is proportional to δ, with $\zeta \approx 0.36\delta$ (Thorpe 1982). Thus, (3.18) and (3.14) can be combined to give the definitive functional form of (3.17) as

$$\frac{\kappa}{d^2N} = \alpha\beta\left(\frac{\omega}{N}\right)^{7/2}\left(\frac{a}{d}\right)^{15/4}\left(\frac{d}{h}\right)^{2}\left(\frac{h}{L_x}\right)\left(\frac{h}{L_y}\right)\left(\frac{h}{H}\right), \tag{3.19}$$

which expresses the dependence of the vertical eddy diffusivity on various governing parameters of the problem at hand.

4. Qualitative observations

An interesting set of qualitative observations were made during the flow evolution around the oscillating body. For all the experiments reported here, the flow field around the cylinder was found to be turbulent as characterized by (i) small-scale inhomogeneities that are evident from shadowgraphs and (ii) inversions observed in the density profiles as obtained by the conductivity probes. Initially, a turbulent boundary layer was found to develop around the cylinder, which then grew laterally until it collapsed owing to buoyancy forces. During the collapse, multiple intrusions were found to form outside the turbulent boundary layer, which then propagated outward into the non-turbulent stratified layer. Such characteristic flows are exemplified by the time sequence of dye-tracer photographs given in figures 2 and 3; in these experiments, the motions fields are highlighted by injecting a dye tracer near the cylinder. The plan view given in figure 2 hints at the presence of strong small-scale turbulent mixing near the cylinder and the dominance of the flow by large-scale bilini (pancake)-like structures at some distances away. Side views of the flow, as observed along the y-direction, are shown in figure 3, and indicate clearly the presence of multiple intrusive features. The formation of such features has been reported by Ivey & Corcos (1982), Thorpe (1982), Browand *et al.* (1987) and Ruddick, McDougall & Turner (1989) in their experiments with oscillating grids in stratified fluids. Thorpe (1982) argued that multiple intrusions are a result of the collapse of turbulence in stratified flows. Browand *et al.* (1987) have proposed that the transport of mixed fluid along the intrusions occurs via propagating solitary waves. In the present study such detailed flow visualizations were not made, in view of the more focused scope of parameterizing bulk mixing characteristics resulting from complex interactions between the topography and the background stratified flow. Stationary conductivity probes placed in the stratified layer away from the cylinder detected internal wave activity. Since the cylinder was oscillated with $\omega/N > 1$, these waves appear to have originated during the collapse of the mixed layer.

Another important feature observed from the dye tracer patterns is the horizontal inhomogeneity of the flow field during the time for which the oscillations are maintained. As the intrusions spread horizontally, return currents (recirculating flows) replenish the 'lost' fluid from the boundary layer. Because of the inhibition of vertical fluid motions due to stratification, the most preferred way of returning fluid into the boundary layer is to set up a recirculating flow in the same horizontal fluid layer, thus minimizing isopycnal displacements. Perhaps for the same reason, large-scale vertical secondary circulations observed by Phillips *et al.* (1986) are also absent in the present

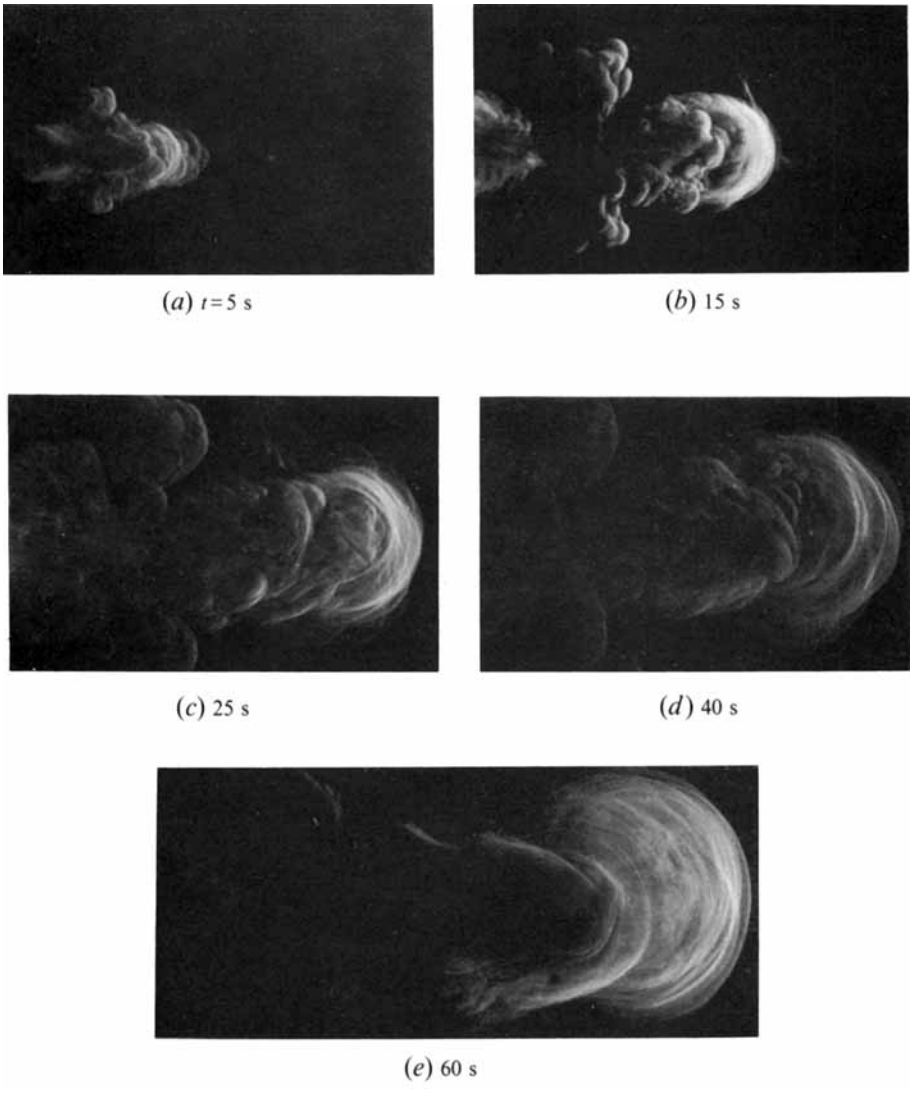

FIGURE 2. Time sequence of photographs showing the evolution of dye tracers injected into the turbulent boundary layer near the cylinder at time $t = 0$. The top view is shown and the flow is illuminated by a horizontal light sheet passing at mid-depth of the cylinder. The parameters are $a/d = 0.4$, $\omega/N = 32$ and $h/H = 0.8$.

case, and the circulation is confined to relatively thin layers. An enlarged schematic view of these flow patterns is shown in figure 4; the flow patterns can be construed as having vertically staggered recirculatory cells, each consisting of an intrusion and a return flow region. In addition, the regions sandwiched between the intrusions have inward velocities which may carry unmixed fluid into the turbulent layer. The circulation patterns around the oscillating cylinder may either be buoyancy driven (intrusions due to mixed-layer collapse) or can occur due to streaming motions that can be developed as a result of unsteady oscillations of the cylinder (e.g. Tatsuno & Bearman 1990). At this point, it is not possible to differentiate between the two and to assess the roles of these two types of circulation.

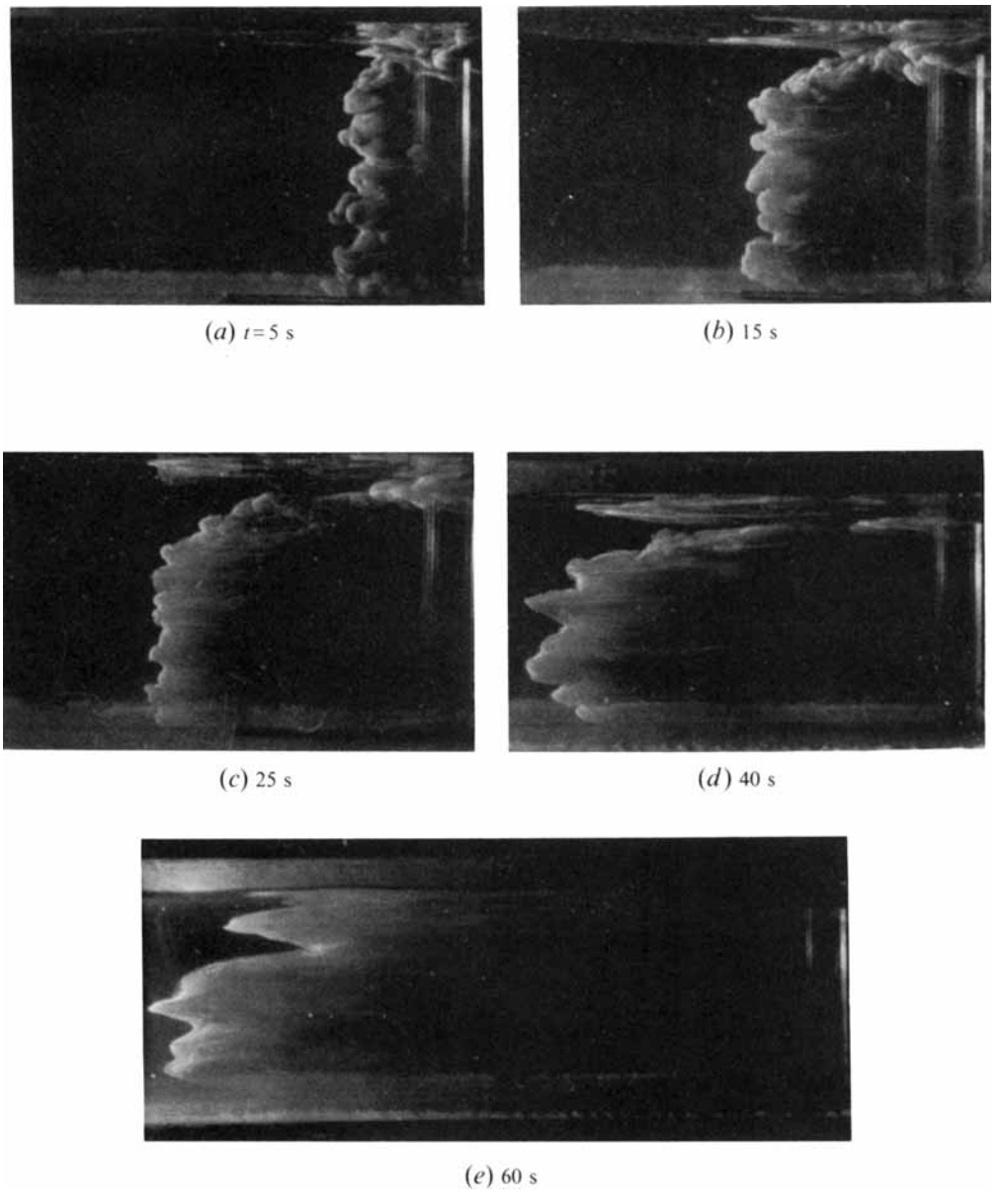

FIGURE 3. Same as figure 2, but the side view is shown.

Figure 5 shows normalized buoyancy profiles taken in rapid succession, from probe 1, at the $(a_1, b_1, \ldots)$ locations shown in figure 1(*b*); similar profiles were obtained from the sequence $(a_2, b_2, \ldots)$ from probe 2. The time between profiles is 60 s, and the first profile was taken 5 min. after the initiation of cylinder oscillations. Note the presence of a small-scale irregular step structure, resulting from the intrusive features. These steps show a very good lateral coherence in the region of probing; however, it is clear that this coherency cannot be expected over the full width of the channel, as is evident from figure 2. The step structure is prominent in the vicinity of the cylinder, but fades away with increased distance from the cylinder. It should be borne in mind that the

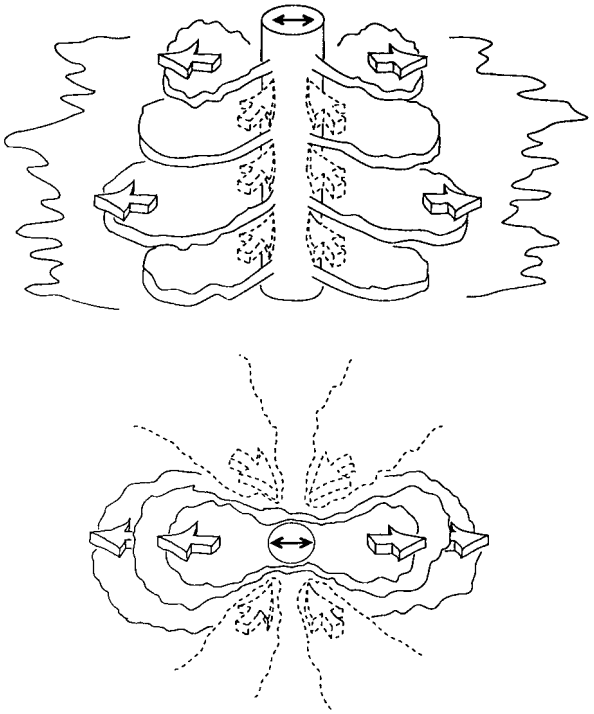

FIGURE 4. A schematic view of intrusive motions. The intrusions and corresponding return currents are mostly generated within layers (at the same azimuths) staggered one atop the other. The regions between the intrusions have a net velocity directed toward the turbulent region.

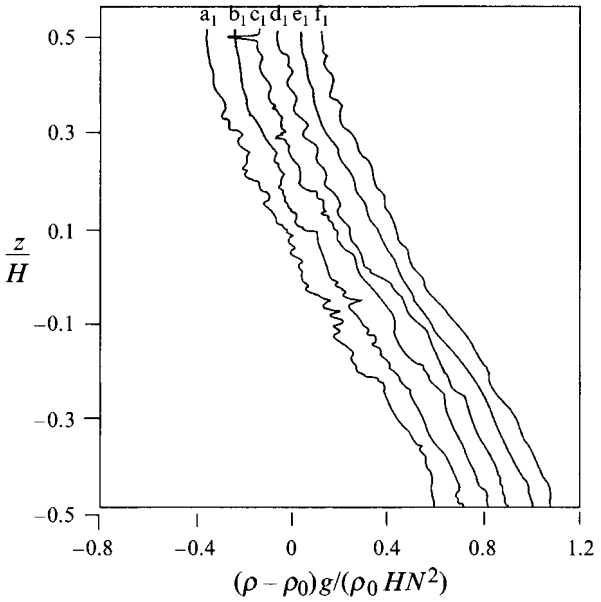

FIGURE 5. Normalized buoyancy profiles obtained from probe 1 at the locations indicated in figure 1(*b*). Profile (a) was taken at approximately $t = 300$ s and each successive profile at 60 s intervals; the parameter values are $a/d = 0.4$, $\omega/N = 32$ and $h/H = 0.8$. Each successive profile (i.e. $b_1, c_1, \ldots$) is displaced 0.1 normalized buoyancy units to the right of the previous profile. Thus, for example, profile (c) should be shifted 0.2 normalized buoyancy units to the left to obtain the specific normalized buoyancy profile.

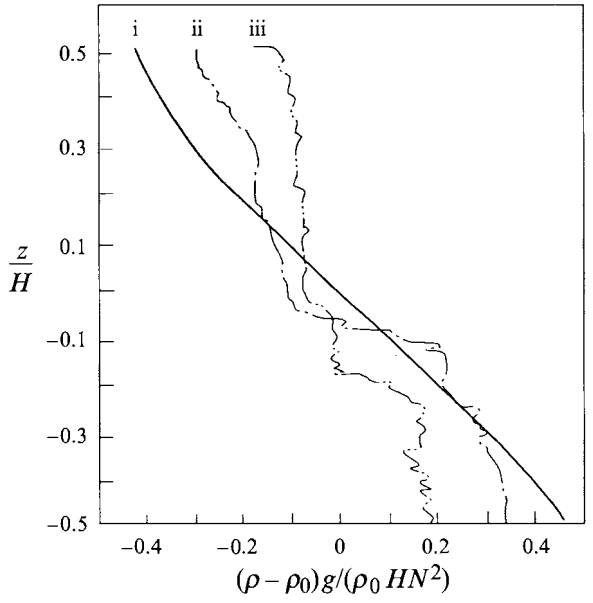

FIGURE 6. A time sequence of normalized buoyancy profiles obtained from probe 1 within the turbulent core. The parameter values are $a/d = 0.4$, $\omega/N = 22$ and $h/H = 0.8$. The times at which the profiles were taken are (i) 0 min, (ii) 5 min, and (iii) 30 min.

density structure away from the cylinder can be modified well before the arrival of the intrusions because of the set up of return flow and the presence of upstream-propagating internal waves which originate at, but propagate faster than, the nose of the intrusions (Manins 1976).

The evolution of the density structure within the turbulent boundary layer was found to depend on the non-dimensional oscillation rate ω/N of the cylinder. At high ω/N, the density gradient decreased rapidly and uniformly (figure 5). However, at lower ω/N, a strong density discontinuity was found to form, approximately at mid-depth of the cylinder (figure 6). Sometimes, at high oscillation speeds, the destruction of the density gradient above the cylinder appears to be rapid; this may be partly due to the turbulence generated by flow separation at the top of the cylinder. In the former case, small-scale density steps are superimposed on the mean gradient, but these are much weaker than the density gradient observed in the latter case. This seemingly paradoxical result – intensification of the density gradient by turbulence – has been discussed theoretically by Phillips (1972) in the context of the formation of density steps in the ocean thermocline and has also been experimentally observed by Ruddick *et al.* (1989). In the present experiments, the localized intensification of the density gradient was observed for experiments carried out with $\omega/N \leqslant 22$. Since the criterion that determines the density evolution patterns is dependent on the other system parameters, the above should not be construed as a rigorous criterion; a more systematic study is required before any conclusions can be made.

Figure 7 shows buoyancy profiles taken 5 minutes after the oscillation of the cylinder has ceased, together with the initial profile (at $t = 0$). The intrusions have now disappeared, presumably by molecular diffusive processes occurring through the interfaces and due to the physical collapse of the mixed fluid within the intrusions (estimates show that molecular diffusive processes can modify the profiles over distances of 0.2 cm or so within this time). A continuous stratification has evolved even

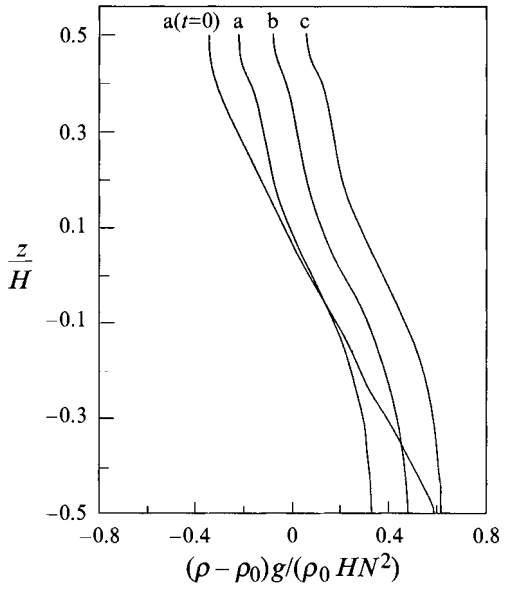

FIGURE 7. Normalized buoyancy profiles obtained from probe 1 at the locations indicated in figure 1(*b*) taken five minutes after the cylinder oscillations ceased: the parameter values are $a/d = 0.4$, $\omega/N = 32$ and $h/H = 0.8$. Profiles (a) and (b) depict the normalized buoyancy against dimensionless depth for the coordinate indicated. Profiles (b) and (c) have been shifted 0.15 and 0.3 normalized buoyancy units to the right. The initial profile ($t = 0$) is also shown.

near the cylinder, due to the readjustments of the intrusive layers following the termination of the forcing. Conductivity profiles taken in the lateral direction from probes ($a_1, a_2, \ldots$) showed a reasonable lateral homogeneity of density over the width of the tank, thus enabling one to use the data of either probe 1 or probe 2 to evaluate the rate of change of potential energy. This lateral homogeneity is also a result of the collapse of the mixed core and the settling of intrusive currents over the entire basin.

Another feature observed with short cylinders with $h/H < 0.6$ is the formation of an upward jet-like flow above the topography; see the time sequence of shadowgraphs shown in figure 8. Presumably, this flow is generated by pronounced vortex shedding present at the summit. Under these conditions, the cylinder oscillations generate a hetrostrophic vortex pair capable of translating upwards, and thus appearing as a jet-like flow. Because of the interest in studying flow around tall seamounts, the experiments reported herein were carried out at $h/H > 0.6$, and studies of $h/H < 0.6$ are noted as a potential future research topic.

5. Quantitative measurements

In order to check the validity of (3.14), or the dependence of κ/d^2N on various parameters given in (3.17), several sets of experiments were performed by changing a single non-dimensional variable while others were being held constant. The buoyancy flux for each experiment was determined by calculating the horizontally averaged density at a given height, measured by traversing conductivity probes, say $\overline{\rho_h}(z, t)$, and then using the finite difference approximation

$$\langle q_3 \rangle \approx \frac{g}{\rho_0 H(\Delta T)} \left[\int_{-H/2}^{H/2} \overline{\rho_h}(z, t_f)\, z\, \mathrm{d}z - \int_{-H/2}^{H/2} \bar{\rho}(z, 0)\, z\, \mathrm{d}z \right], \tag{5.1}$$

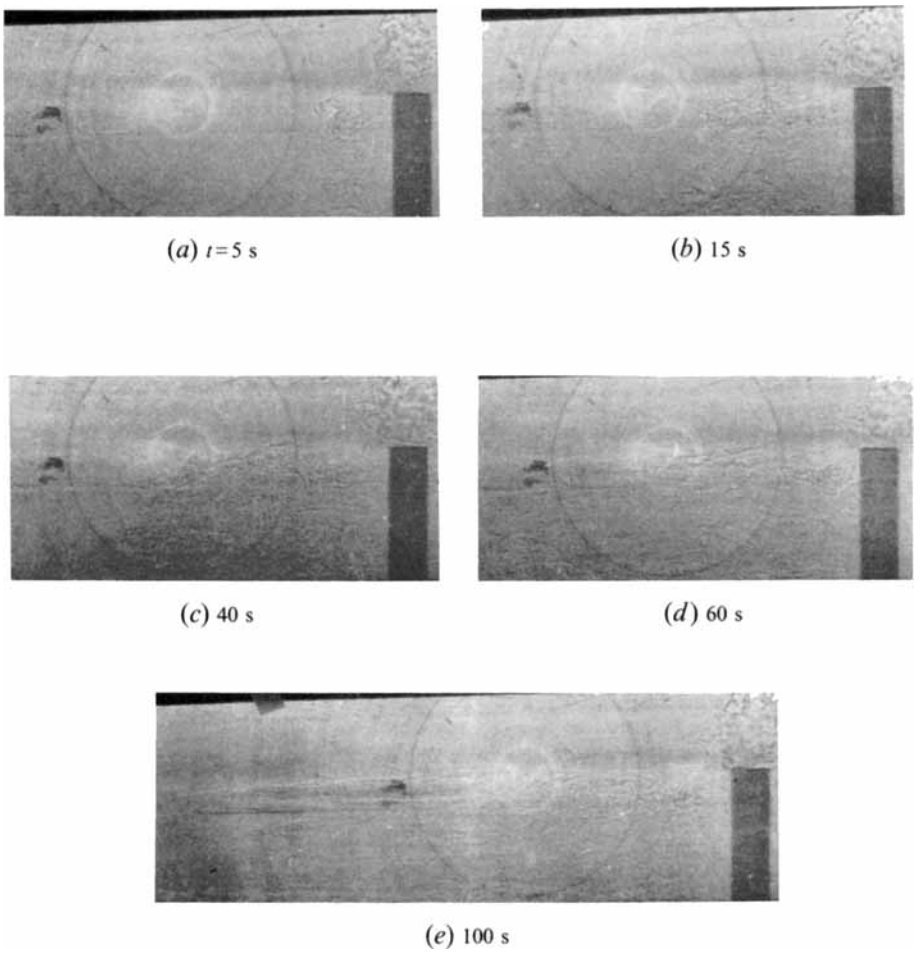

FIGURE 8. A time sequence of shadowgraphs that depict the generation of an upward jet from the summit of the cylinder. The experimental parameters are $a/d = 0.4$, $\omega/N = 22$ and $h/H = 0.6$.

where $\Delta T(= t_f)$ is the duration of oscillation of the cylinder, $\overline{\rho_h}(z, t_f)$ is the final horizontally averaged density at z and $\bar{\rho}(z, 0)$ is the horizontally homogeneous density distribution before starting the cylinder oscillations. As noted previously, $\overline{\rho_h}(z, t_f)$ was measured about 5 minutes after the halting of the cylinder, allowing intrusive motions to settle to their equilibrium density levels. The density measurements were taken at various locations shown in figure 1(*b*), and the horizontal average was taken to calculate $\overline{\rho_h}(z, t)$.

Figure 9(*a*) shows the variation of the normalized eddy diffusivity with the frequency ratio ω/N, with all other non-dimensional parameters of (3.17) held constant. Note the good agreement between the data and the $(\omega/N)^{7/2}$ behaviour predicted by (3.19) (solid line); the 7/2 slope, however, is not the best-fit line. Similarly, figure 9(*b*) shows the variation of κ/d^2N versus a/d, while the other parameters are held constant; the agreement with the power-law prediction $(a/d)^{15/4}$ is good. Figure 9(*c*) shows the variation of κ/d^2N with d/h; again there is good agreement with the analysis.

A few other experiments were also performed changing h and H, but due to practical limitations, their variations were in a limited parameter range. The results of all

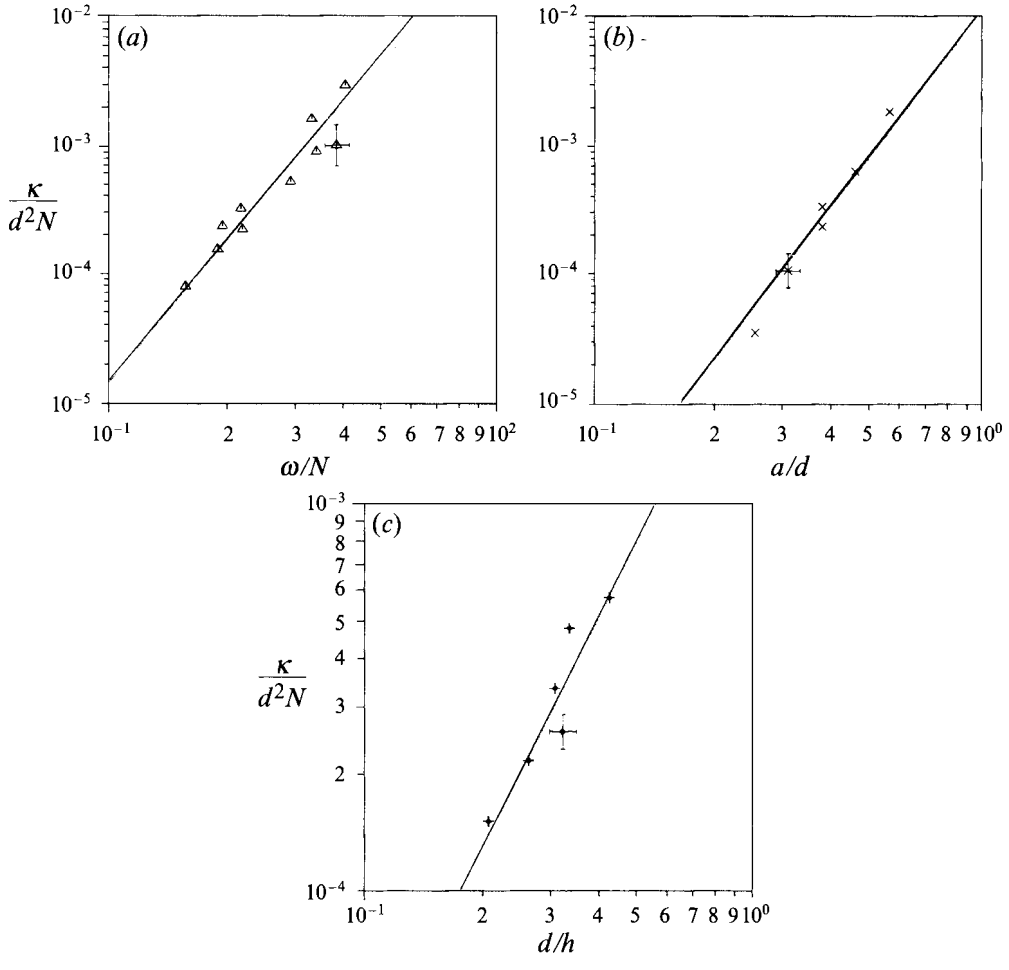

FIGURE 9. Variation of normalized eddy diffusivity: (*a*) with non-dimensional oscillation frequency ω/N ($a/d = 0.4$, $d/h = 0.18$), (*b*) with a/d ($\omega/N \approx 22$, $d/H = 0.18$) and (*c*) with d/h ($\omega/N = 22$, $a/d = 0.4$). $h/H = 0.8$.

experiments are presented in figure 10, as a log–log plot of κ/d^2N versus the parameter $(\omega/N)^{7/2}(a/d)^{15/4}(d/h)^2(h/L_x)(h/L_y)(h/H)$. The best-fit line to the data has a slope of 0.98 with a correlation coefficient of 0.93, indicating support for the formulations (3.19) and (3.14). The results can be expressed as

$$\frac{\kappa}{d^2N} = 8\times 10^{-5}\left(\frac{\omega}{N}\right)^{7/2}\left(\frac{a}{d}\right)^{15/4}\left(\frac{d}{h}\right)^2\left(\frac{h}{L_x}\right)\left(\frac{h}{L_y}\right)\left(\frac{h}{H}\right), \tag{5.2}$$

for experiments carried out in the parameter ranges $13 < \omega/N < 42$, $0.26 < a/d < 0.58$, $0.18 < d/h < 0.49$, $0.6 < h/H < 0.85$, $0.064 < h/L_x < 0.116$ and $0.2 < h/L_y < 0.36$. Satisfactory collapse of the data for $\omega/N < 22$ and $\omega/N > 22$ cases indicate that the bulk mixing characteristics may be insensitive to the details of flow evolution near the cylinder.

Because mixed fluid formed near the boundaries is carried into the stratified basin by intrusive motions, it is of interest to note the behaviour of such intrusions. These intrusions are formed as a consequence of the collapse of the turbulent boundary layer

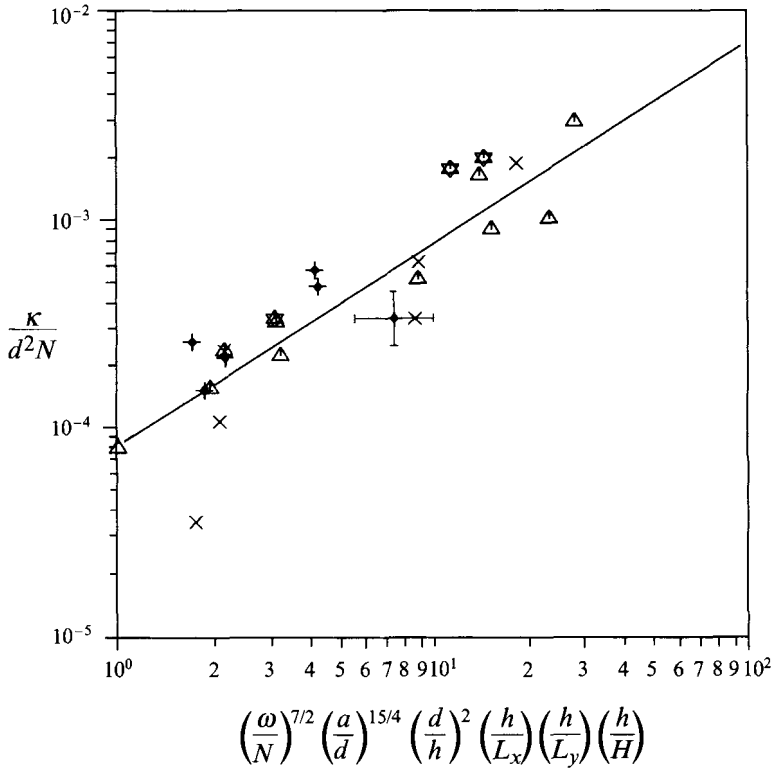

FIGURE 10. All available data are plotted to check the validity of (3.19).

(Thorpe 1982), and the position of their frontal location can be written in terms of the properties of the turbulent region and the outside stratification as

$$x_f = f_1(l, u, N, t) \tag{5.3}$$

or

$$\frac{x_f}{l} = f_2\left(Nt, \frac{u}{Nl}\right), \tag{5.4}$$

where u and l are the r.m.s. velocity and the integral lengthscale of the turbulence, respectively, $f_1, f_2, \ldots$ are functions and t is the time. The influence of the viscosity has been neglected by assuming fully developed turbulence within the boundary layer and the inertia–buoyancy force balance within the intrusions during their initial spreading (Manins 1976). Since u/Nl can be considered as constant within the turbulent boundary layer (Browand & Hopfinger 1985; Thorpe 1982; Browand *et al.* 1987), (5.4) simply implies $x_f/l = f_3(Nt)$. According to Thorpe (1982) and Browand & Hopfinger (1985), the integral scale within the turbulent region is of the same order as the width of the boundary layer δ given in (3.18), and the mean thickness of the intrusions is proportional to δ.

Figure 11 shows the variation of (x_f/δ) with Nt. Results support a power-law behaviour of the form

$$x_f/\delta = 0.018(Nt), \tag{5.5}$$

for $Nt < 30$. As is evident from figure 3, different intrusions (at different vertical levels) tend to propagate at somewhat different rates and, in presenting the results, vertically

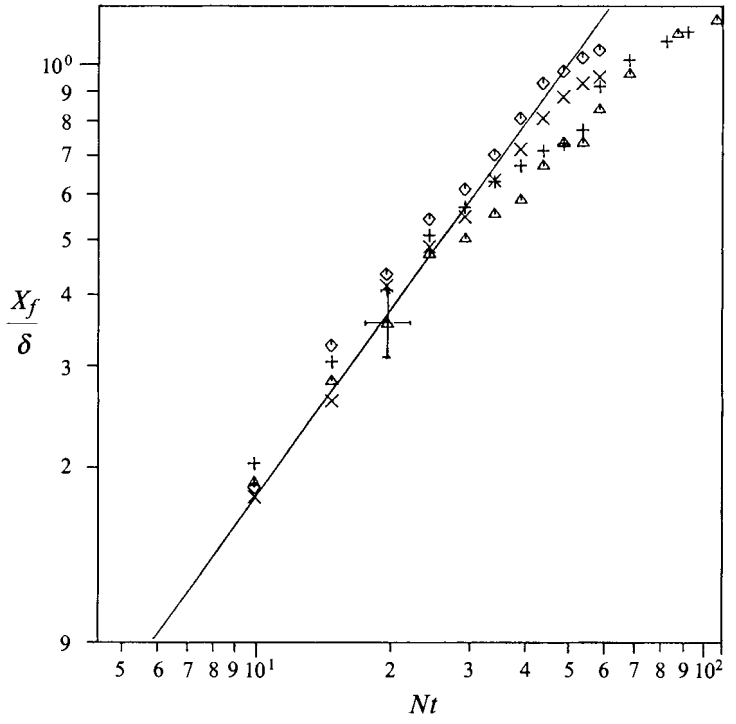

FIGURE 11. Dimensionless position of the intrusion nose against the dimensionless time; the parameter values are $a/d = 0.4$ and $h/H = 0.8$.

averaged positions of the leading edges of the intrusions have been used. The experimental results show no systematic dependence on h/H.

6. Summary

In the foregoing sections, the results of an experimental study directed at parameterizing turbulent mixing induced by oscillatory stratified flow past a right circular cylinder were presented. In the experiments, the cylinder was oscillated in a fluid that was otherwise at rest with respect to its surroundings. The work was motivated by observations made during two recent field oceanography programs that the background flow near the seamounts under consideration was, to a good approximation, oscillatory (i.e. of a purely tidal nature). Although the bathymetry of seamounts as well as the turbulent boundary layers around them are complex, as a first step toward modelling them, a right circular cylinder was used. The principle results of this study are as follows.

(i) The interaction between the topography and the flow leads to the generation of an isolated turbulent region (turbulent core), within which active turbulent mixing takes place. The evolution of the stratification within the core depends on the nature of the turbulence and the strength of the stratification. At high turbulent intensities, the core tends to get mixed by uniformly decreasing its buoyancy gradient, whereas at lower turbulent intensities a sharp single density interface, separated by two mixed regions, can be formed. Analogous observations have been made in some previous experiments, for example Ruddick *et al.* (1989).

(ii) The flow patterns at the summit of the cylinder were dependent on h/H,

where h and H are the height of the cylinder and the water depth, respectively. When $h/H \lesssim 0.6$, an upward jet is formed at the top of the obstacle. When $h/H \gtrsim 0.85$, considerable surface wave motion developed.

(iii) Gravitational collapse of the turbulent core generates a series of intrusions carrying mixed fluid into the surroundings in much the same way as reported by Ivey & Corcos (1982). Thereafter, the flow is bi-directional with intrusions feeding mixed fluid into the interior of the basin and return currents carrying interior stratified fluid into the core. Diapycnal mixing takes place effectively in the turbulent core, but exchange of this mixed fluid with the non-turbulent interior makes this localized mixing equivalent to much weaker basin-scale mixing.

(iv) The density structure in the vicinity of the obstacle was found to be laterally coherent. Across the intrusive fronts, the microstructure is obviously inhomogeneous. Internal waves were found to be present outside the intrusions; these appear to be a consequence of the release of potential energy during the gravitational collapse of mixed fluid at the edge of the turbulent core (cf. Wu 1969).

(iv) The net effect of mixing in the turbulent core, which is communicated to the basin via intrusions, is the increase of the potential energy of the fluid mass. An expression was derived to relate the rate of potential energy increase of the basin to the basin-averaged buoyancy flux associated with mixing.

(vi) The basin-scale vertical eddy diffusivity was calculated by measuring the average rate of increase of potential energy and the results were found to be in good agreement with a simple model based on the energetics of the system. The expression for the eddy diffusivity is

$$\kappa/d^2N \approx 8\times 10^{-5}\left(\frac{\omega}{N}\right)^{7/2}\left(\frac{a}{d}\right)^{15/4}\left(\frac{d}{h}\right)^{2}\left(\frac{h}{L_x}\right)\left(\frac{h}{L_y}\right)\left(\frac{h}{H}\right),$$

or

$$\kappa/d^2N = 1\times 10^{-4}Ri^{-1.5}(d/H)\,(\delta h/L_x L_y),$$

where d is the diameter of the cylinder, N is the background stratification, ω and a are the frequency and amplitude of cylinder oscillations, respectively, δ is the thickness of the turbulent boundary layer, $Ri = N^2d^2/a^2\omega^2$ is a bulk Richardson number, and L_x and L_y are the length and width of the basin.

(vii) The initial propagation of intrusions appears to be governed by an inertia–buoyancy force balance, for example as in Broward *et al.* (1987). The spreading occurs according to $x_f/\delta \approx 0.018(Nt)$, where x_f is the frontal horizontal coordinate and t is the time elapsed after the initiation of the oscillatory motion.

7. Discussion

As stated, the aim of the reported work was to obtain a parameterization for the basin-scale diapycnal diffusivity pertinent to mixing induced by oscillatory fluid flow past a right-circular submerged cylinder in a stratified fluid. Thus, no detailed probing into fundamental mixing mechanisms near the obstacle was made, although some of them were evident from overall measurements. One such observation is the localized sharpening of the buoyancy gradient in the turbulent core, when the frequency of oscillations is less than a critical value, although turbulent mixing is active in the core. This observation is in consonance with the prediction of Phillips (1972) that under certain conditions a linearly stratified region transporting a uniform buoyancy flux can generate, via an instability mechanism, sharp density gradients. Posmentier (1977) has also proposed a similar mechanism.

The instability mechanism of Phillips (1977) comes into effect when the non-dimensional eddy diffusivity $G(Ri_g)$, defined by

$$\kappa = u_*^2 N^{-1} G(Ri_g) = u_*^2 u_z^{-1} Ri_g^{-1/2} G(Ri_g),$$

decreases faster than $Ri_g^{-1/2}$ at sufficiently large Ri_g; here u_* is a friction velocity, u_z is the vertical velocity shear and Ri_g is the gradient Richardson number, $Ri_g = N^2/u_z^2$. When this criterion is satisfied, local intensification of the density gradient was predicted when Ri_g exceeds a critical value. Recently, Ruddick *et al.* (1989) have demonstrated the viability of Phillips' mechanism, by demonstrating the formation of step microstructure when a linearly stratified fluid is agitated by an oscillating array of rods, whence the oscillating frequency is low. Although their experiment did not include such elements as mean shear and horizontal inhomogeneity used in Phillips' derivation, their observations are considered as a clear demonstration of a 'zero-mean-flow' equivalent of the Phillips' mechanism. The present experiment also lacks a mean flow in that no Ri_g can be identified; yet it demonstrates the possibility of the intensification of density gradient at low oscillating frequencies, or equivalently, large Ri_g. If it is assumed that Ri_g is a monotonically increasing function of Ri, then the formation/non-formation of steps should be dependent on the bulk Richardson number $Ri = N^2 d^2/a^2\omega^2$. Further work is necessary to understand the role of Ri in the evolution of the density microstructure near the obstacle.

In spite of the aim of modelling oceanic seamount-induced mixing, the vast difference between the two situations should be borne in mind in extrapolating the present results to oceanic cases. For example, oscillation of the cylinder may not truly represent the oscillatory flow past a stationary obstacle because of the generation of a bottom boundary layer in the latter case. Near seamounts, although the flow can be oscillatory, a mean component of the motion can be present, which may enhance shear and turbulence (see the discussions by Roden 1991; Gibson, Nabatov & Ozmidov 1994). Because of the large horizontal scale of the seamount, the distribution of mixed fluid in the basin is bound to be affected by the Earth's rotation, although mixing near the seamount may still be independent of Coriolis effects (e.g. Ivey 1987). Another important aspect is the slope of the boundaries of the seamount which is an additional governing parameter for the problem (for example, see Salmun, Killworth & Blundell 1991 and Salmun & Phillips 1972). McDougall (1989) pointed out that the change of the thickness of the boundary layer around the seamount can generate a sinking dia-neutral velocity near the seamount, which may lead to a flow convergence zone. Change of the turbulence intensity with height is also another matter of concern, as it changes the diffusivity along the boundary. Sloping boundaries are susceptible to additional mixing mechanisms such as resonant breaking of reflecting internal waves (Eriksen 1982; Garrett 1991). Much work remains to be done before a reasonable understanding of the mixing mechanisms at seamounts can be obtained.

In modelling the oceanic circulation, it is imperative to have a reasonable estimate of the effective eddy diffusivity. Earlier formulations, such as that of Stommel & Arons (1960), have been based on spatially uniform upwelling driven by interior mixing in the basin. Following Armi (1978), an alternative view exists that mixing is confined principally to boundaries with the mixed fluid being introduced into the ocean interior as described above. This concept demands equivalent basin-averaged eddy diffusivities, based on boundary mixing events, and this was the theme of the present work.

The authors wish to thank Leonard Montenegro, I. P. DeSilva, C. Y. Ching, S.

Fonseka, Y. Noh, G. Oth and X. Zhang for their help in numerous ways. This work was supported by the office of Naval Research (Small-scale/Meso-scale/Arctic programs) and the National Science Foundation through research contracts/grants to D. L. Boyer and H. J. S. Fernando.

REFERENCES

ARMI, L. 1978 Some evidence for boundary mixing in deep ocean. *J. Geophys. Res.* **83**, 1971–1979.

BRINK, K. H. 1990 On the generation of seamount trapped waves. *Deep-Sea Res.* **37**, 1569–1582.

BROWAND, F. K., GUYOMAR, D. & YOON, S.-C. 1987 The behaviour of a turbulent front in a stratified fluid: Experiment with an oscillating grid. *J. Geophys. Res.* **92**, 5329–5341.

BROWAND, F. K. & HOPFINGER, E. J. 1985 The inhibition of vertical turbulence scale by stable stratification. In *Turbulence and Diffusion in Stable Environments* (ed. J. C. R. Hunt), pp. 15–27. Clarendon.

COLEMAN, H. W. & STEELE, W. G. JR 1989 *Experimentation and Analysis for Engineers.* Wiley.

D'ASARO, E. A. & MORISON, J. H. 1992 Internal waves and mixing in the Arctic ocean. *Deep-Sea Res.* **39**, suppl. 2, S459–484.

DILLON, T. R., MOUM, J. N., CHERESKIN, T. K. & CALDWELL, D. R. 1989 Zonal momentum balance at the equator. *J. Phys. Oceanogr.* **19**, 1561–1570.

ERIKSEN, C. C. 1982 Observations of internal wave reflection off sloping bottoms. *J. Geophys. Res.* **87**, 525–538.

FORTUIN, T. 1960 Theory and application of two supplementary methods of generating density gradient columns. *J. Polymer Sci.* **44**, 505–515.

GARRETT, C. 1989 Are diapycnal fluxes linked to lateral stirring rates? In *Proc. Fifth 'Aha Huliko' a Hawaiian Winter Workshop on Parameterization of Small Scale Process, Hawaii Institute of Geophysics, Honolulu*, pp. 317–327.

GARRETT, C. 1991 Marginal mixing theories. *Atmos. Oceans* **29**, 313–339.

GARRETT, C., MACCREADY, P. & RHINES, P. 1993 Boundary mixing and arrested Ekman layers; Rotating stratified flow near a sloping boundary. *Ann. Rev Fluid Mech.* **25**, 291–323.

GIBSON, C. H., NABATOV, V. & OZMIDOV, R. 1994 Measurements of turbulence and fossil turbulence near Ampere seamounts. *Dyn. Atmos. Oceans* **19**, 175–204.

GREGG, M. C. 1989 Scaling turbulent dissipation in the thermocline. *J. Geophys. Res.* **94**, 9686–9698.

HEAD, M. J. 1983 The use of four-electrode conductivity probes for high resolution measurement of turbulent density or temperature variation in salt-stratified water flows. PhD dissertation, University of California, San Diego.

IMBERGER, J. & IVEY, G. 1993 Boundary mixing in stratified reservoirs. *J. Fluid Mech.* **248**, 477–491.

IVEY, G. N. 1987 The role of boundary mixing in the deep ocean. *J. Geophys. Res.* **92**, 11873–11878.

IVEY, G. N. & CORCOS, G. M. 1982 Boundary mixing in stratified fluids. *J. Fluid. Mech.* **121**, 1–26.

KILLWORTH, P. D. 1976 The mixing and spreading Phases of MEDOC. *Prog. Oceanogr.* **7**, 59–90.

MANINS, P. C. 1976 Intrusions into stratified fluids. *J. Fluid. Mech.* **74**, 547–560.

MCDOUGALL, T. J. 1989 Dianeutral advection. In *Proc. Fifth 'Aha Huliko' a Hawaiian Winter Workshop on Parameterization of Small Scale Processes, Hawaii Institute of Geophysics, Honolulu*, pp. 289–315.

MCEWAN, A. D. 1983 The kinematics of stratified mixing through internal wave breaking. *J. Fluid Mech.* **128**, 47–58.

MUNK, W. H. 1966 Abyssal recipes. *Deep-Sea Res.* **13**, 707–730.

OSBORN, T. R. 1980 Estimates of the local rate of vertical diffusion from dissipation measurements. *J. Phys. Oceanogr.* **10**, 83–89.

OZMIDOV, R. V. 1990 A study of eddies and turbulence near Ampere Seamount. *Theses of 3rd All Union Conf. on Eddies and Turbulence in the Ocean, Kaliningrad, USSR*, pp 37–90.

PHILLIPS, O. M. 1972 Turbulence in strongly stratified fluids – is it unstable? *Deep-Sea Res.* **19**, 79–81.

PHILLIPS, O. M. 1977 *Dynamics of the Upper Ocean.* Cambridge University Press.

PHILLIPS, O. M., SHYU, J.-H. & SALMUN, H. 1986 An experiment on boundary mixing. *J. Fluid. Mech.* **173**, 473–499.

POSMENTIER, E. S. 1977 The generation of salinity fine structure by vertical diffusion. *J. Phys. Oceanogr.* **7**, 292–300.

RODEN, C. J. & TAFT, B. A. 1985 Effect of Emperor seamounts on the mesoscale thermohaline structure during the summer of 1982. *J. Geophys. Res.* **90** (C1), 839–855.

RODEN, G. I. 1991 Mesoscale flow and thermohaline structure around Fieberling Seamount. *J. Geophys. Res.* **96**, 16653–16672.

RUDDICK, B. R., MCDOUGALL, T. J. & TURNER, J. S. 1989 The formation of layers in a uniformly stratified density gradient. *Deep-Sea Res.* **36**, 597–609.

SALMUN, H., KILLWORTH, P. D. & BLUNDELL, J. R. 1991 A two dimensional model of boundary mixing. *J. Geophys. Res.* **96** (C10), 18447–18474.

SALMUN, H. & PHILLIPS, O. M. 1992 An experiment on boundary mixing. Part 2. The slope dependence at small angles. *J. Fluid Mech.* **240**, 355–377.

STOMMEL, H. & ARONS, A. B. 1960 On the abyssal circulation of the world ocean. I. Stationary planetary flow patterns on a sphere. *Deep-Sea Res.* **6**, 140–154.

TATSUNO, M. & BEARMAN, P. W. 1990 A visual study of the flow around an oscillating circular cylinder at low Keulegan–Carpenter numbers and low Stokes numbers. *J. Fluid Mech.* **211**, 157–182.

THORPE, S. A. 1982 On the layers produced by rapidly oscillating a vertical grid in a uniformly stratified fluid. *J. Fluid. Mech.* **124**, 361–375.

THORPE. S. A. 1987 Current and temperature variability on the continental slope. *Phil. Trans. R. Soc. Lond.* A **323**, 427–517.

TURNER, J. S. 1985 Multicomponent convection. *Ann. Rev. Fluid Mech.* **17**, 11–44.

WOODS, A. W. 1991 Boundary-driven mixing. *J. Fluid Mech.* **226**, 625–654.

WU, J. 1969 Mixed region collapse with internal-wave generation in a density stratified medium. *J. Fluid Mech.* **35**, 531–544.